ADVANCED FUNCTIONAL MATERIALS
www.afm-journal.de

# Toward Sustainability in All-Printed Accumulation Mode Organic Electrochemical Transistors

*Anatolii Makhinia, Lize Bynens, Arwin Goossens, Jasper Deckers, Laurence Lutsen, Koen Vandewal, Wouter Maes, Valerio Beni, and Peter Andersson Ersman**

**This study reports on the first all-printed vertically stacked organic electrochemical transistors (OECTs) operating in accumulation mode; the devices, relying on poly([4,4′-bis(2-(2-(2-methoxyethoxy)ethoxy)-2,2′-bithiophen-5,5′-diyl]-*alt*-[thieno[3,2-*b*]thiophene-2,5-diyl]) (pgBTTT) as the active channel material, are fabricated via a combination of screen and inkjet printing technologies. The resulting OECTs ($W/L \approx 5$) demonstrate good switching performance; $g_{m,\,norm} \approx 13$ mS cm$^{-1}$, $\mu C^* \approx 21$ F cm$^{-1}$ V$^{-1}$ s$^{-1}$, ON–OFF ratio $> 10^4$ and good cycling stability upon continuous operation for 2 h. The inkjet printing process of pgBTTT is established by first solubilizing the polymer in dihydrolevoglucosenone (Cyrene), a non-toxic, cellulose-derived, and biodegradable solvent. The resulting ink formulations exhibit good jettability, thereby providing reproducible and stable p-type accumulation mode all-printed OECTs with high performance. Besides the environmental and safety benefits of this solvent, this study also demonstrates the assessment of how the solvent affects the performance of spin-coated OECTs, which justifies the choice of Cyrene as an alternative to commonly used harmful solvents such as chloroform, also from a device perspective. Hence, this approach shows a new possibility of obtaining more sustainable printed electronic devices, which will eventually result in all-printed OECT-based logic circuits operating in complementary mode.**

## 1. Introduction

In recent decades, the rise of Printed Electronics (PE) has been triggered by the large selection of solution-processible materials and low-cost fabrication technologies allowing complex form factors, e.g., soft, stretchable, bendable, etc. As a result, PE has enabled new frontiers and breakthroughs in healthcare by linking electronics with biology, hybrid electronics, agriculture, etc.[1] However, from a manufacturing point of view, toxic solvents are one of the major concerns in the preparation of inks, pastes, and slurries used for the additive manufacturing of electronic devices. The next-generation sustainable PE should address these challenges using organic, biodegradable, solution-processible materials and non-toxic solvents to fabricate organic electronic devices to reduce electronic waste and ensure safe human usage.[2,3] The organic electrochemical transistor (OECT) technology holds promise for all-printed organic logic circuits,[4–7]

A. Makhinia, V. Beni, P. Andersson Ersman
RISE Research Institutes of Sweden
Digital Systems
Smart Hardware, Printed, Bio- and Organic Electronics
Norrköping 60233, Sweden
E-mail: peter.andersson.ersman@ri.se

A. Makhinia
Laboratory of Organic Electronics
Department of Science and Technology
Linköping University
Norrköping 60221, Sweden

L. Bynens, J. Deckers, L. Lutsen, W. Maes
Institute for Materials Research (IMO-IMOMEC)
Design & Synthesis of Organic Semiconductors (DSOS)
Hasselt University
Diepenbeek 3590, Belgium

A. Goossens, K. Vandewal
Institute for Materials Research (IMO-IMOMEC)
Organic Opto-Electronics (OOE)
Hasselt University
Diepenbeek 3590, Belgium

J. Deckers, L. Lutsen, K. Vandewal, W. Maes
Interuniversity Microelectronics Centre (IMEC)
Associated Lab IMOMEC
Diepenbeek 3590, Belgium

The ORCID identification number(s) for the author(s) of this article can be found under https://doi.org/10.1002/adfm.202314857



**DOI: 10.1002/adfm.202314857**

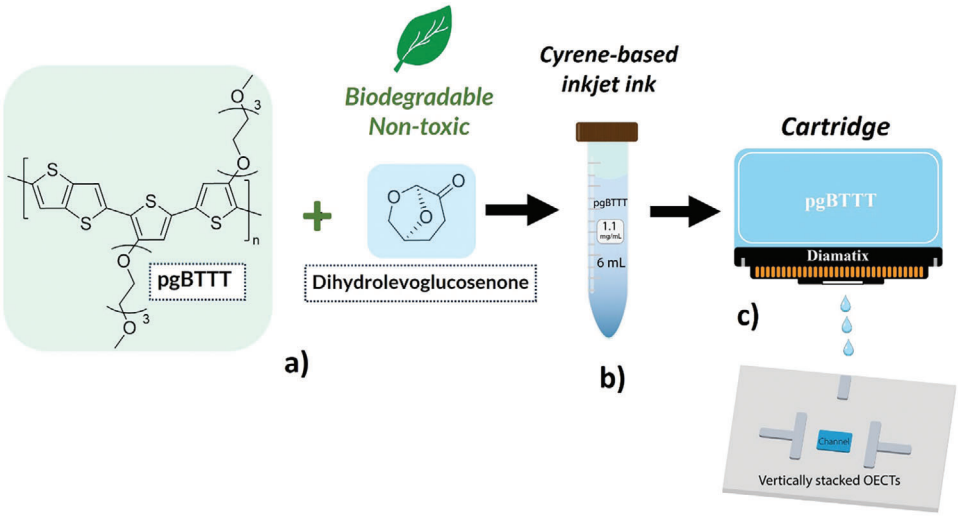


**Figure 1.** Ink preparation scheme for the pgBTTT-based inkjet printable ink. a) Chemical structures of pgBTTT and Cyrene, b) inkjet ink based on pgBTTT dissolved in Cyrene, c) schematic illustration of an inkjet cartridge filled with pgBTTT ink to enable inkjet printing of the channels in vertically stacked OECTs.

electrophysiological monitoring,[8–11] biological sensors[12–15] and neuromorphic devices.[16] The selection of the relevant printing technology will dictate the performance of the electronic devices, e.g., OECTs, and their integration on different substrates.[17–20] An OECT is a three-terminal device comprising gate, source, and drain electrodes.[21] The source and drain electrodes are electronically connected via a semiconducting material, forming the so-called transistor channel, which is also ionically linked with the gate electrode through an electrolyte layer. Depending on the application, the electrolyte may be deposited manually or by printing techniques, and it may be liquid or curable into a solidified form. The gate electrode is either located in the same plane as the transistor channel (lateral or co-planar OECT) or printed on top of the electrolyte layer, forming vertically stacked OECT architectures. The selection of the channel material determines the transistor type and operation mode, i.e., p- or n-type and depletion or accumulation mode devices.[22,23]

The synthesis of novel solution-processable p- and n-type organic semiconductor materials and the design of simple device architectures have fostered the development of microfabricated and even printable OECTs governed by low voltage operation (< 1 V) in solid or liquid electrolytes.[24,25] In addition, the transport of charges occurs within the entire bulk of the channel material, giving rise to high volumetric capacitance and high current levels, which typically results in high transconductance and high ON–OFF ratios along with a prolonged switching time as compared to most other transistor technologies. The latter is due to the relatively slow ion migration to/from the organic semiconducting channel material as a function of the applied gate voltage.[26]

The performance of the OECT will also depend on the device architecture, e.g., vertically stacked or co-planar arrangement, and processing parameters (curing, sintering, UV light intensity) of the respective layer of the device. As a result, the OECT performance can be improved by the selection of fabrication technology, choice of materials, and device architectures. Using appropriate processing steps for the deposition and curing of inks/materials is, therefore, vital to ensure optimized OECT performances and reproducible devices.[27]

In this work, we demonstrate the first all-printed p-type accumulation mode OECTs wherein the active layers (channel, electrolyte, and gate electrodes) are vertically stacked on top of each other; a device architecture that allows for shorter switching time and reduced device footprint. High-performing OECTs manufactured by microfabrication (feature sizes ≈10 µm) with pgBTTT (poly([4,4′-bis(2-(2-(2-methoxyethoxy)ethoxy)ethoxy)−2,2′-

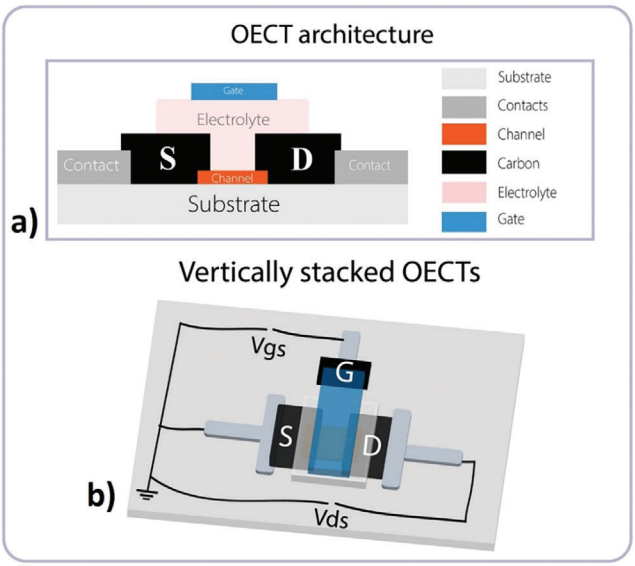


**Figure 2.** Schematic illustration of a typical vertically stacked OECT architecture, here employing pgBTTT as the channel material. Illustrations showing the a) cross–section view and b) top view of a typical vertically stacked OECT architecture.

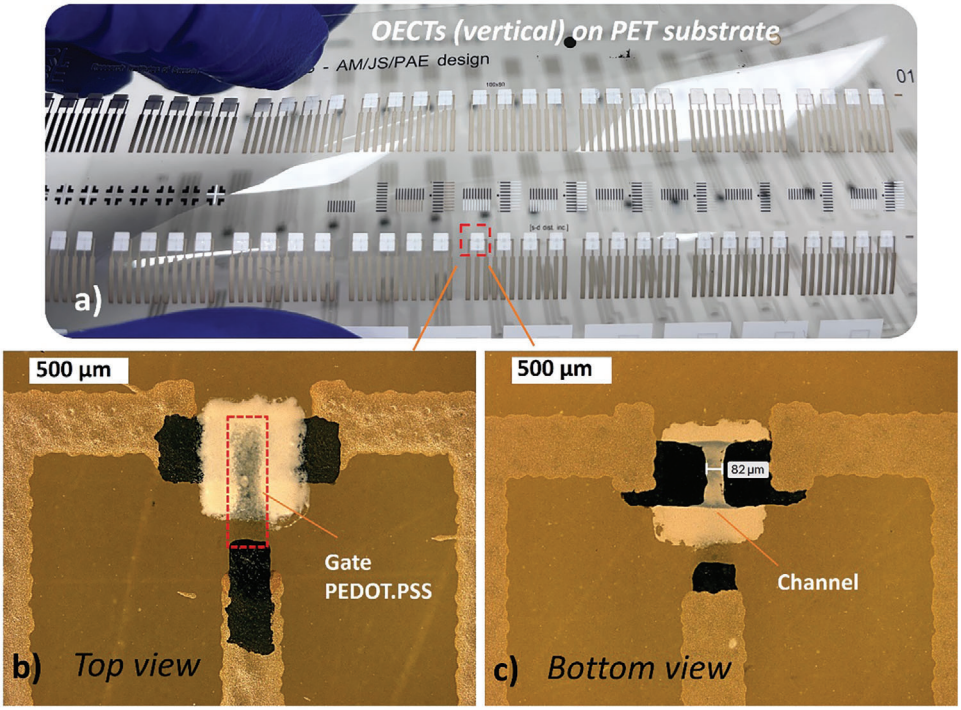


**Figure 3.** All-printed vertically stacked OECTs. a) Photograph showing OECTs printed on top of a PET substrate. The microscope images show the b) top and c) bottom (through the substrate) views of the all-printed vertically stacked OECTs.

bithiophen-5,5′-diyl]-*alt*-[thieno[3,2-*b*]thiophene-2,5-diyl])) serving as the channel material have been previously reported. The excellent performance was attributed to an increase in hole mobility, explained by optimized side-chain interactions due to the highly ordered structure.[28–30] The photolithographic process of fabricating these OECTs relied on drop-casting a pgBTTT-based solution from chloroform. The most recent work (2023) demonstrated photo-responsive OECTs created via pre-patterned Au electrodes and drop-cast solutions of pgBTTT blended with other materials, also dissolved in chloroform.[31]

This study reports on the combination of printing technologies to create all-printed accumulation mode OECTs. The p-type semiconducting conjugated polymer pgBTTT was inkjet printed to create the OECT channels, while the remaining layers were screen printed to complete the vertically stacked OECT devices. The bio-based and biodegradable solvent dihydrolevoglucosenone (Cyrene) was employed to dissolve the polymer and formulate the pgBTTT-based inkjet ink. The use of Cyrene for the ink preparation of the OECT channel material has not yet been reported. The application of biodegradable and non-toxic solvents, as an alternative to chloroform, is essential in additive fabrication, e.g., inkjet printing, to allow industrial-scale manufacturing, to decrease the environmental impact of processes and the preparation of materials, and to ensure a safe working environment upon usage. As a result, high-performing, vertically stacked, reproducible, and stable p-type accumulation mode all-printed OECTs were fabricated to be further utilized as circuits in various sustainable PE applications, eventually targeting all-printed circuits operating in complementary mode.

Additionally, this work evaluates the effects of the solvent on the electrical performance of conventional spin-coated OECTs (Au-based source and drain electrodes, Ag/AgCl gate electrode, and aqueous 0.1 mM NaCl electrolyte), which justifies the choice of Cyrene as a replacement for other harmful solvents also from a device perspective, besides the benefits related to safety and the environment.

## 2. Results and discussion

### 2.1. Chemical Synthesis

The pgBTTT polymer was prepared via an adapted literature procedure.[30] Details on the synthetic procedure can be found in the Experimental section. After synthesizing the polymer, the crude mixture was treated with a palladium (Pd) scavenger, diethylammonium diethyldithiocarbamate, since it has been reported that residual Pd, originating from the $Pd_2(dba)_3$ catalyst used for the polymerization, may have a negative impact on the device performance.[32] To get an idea about the molecular weight of the polymer, matrix-assisted laser desorption ionization time-of-flight (MALDI-ToF) mass spectrometry was carried out on the chloroform fraction of pgBTTT after Soxhlet extractions, see the Experimental section.

### 2.2. Ink Formulation

Herein, an inkjet ink was prepared by dissolving the conjugated polymer pgBTTT (≈1.1 mg $mL^{-1}$) in dihydrolevoglucosenone

(Cyrene) at ambient conditions (see **Figure 1a**). Cyrene, a solvent with high boiling point (227 °C) and high density (1.25 g $mL^{-1}$), allows for the preparation of viscous inks (> 15 cP) at low semiconductor concentrations (≈1 mg $mL^{-1}$) to facilitate inkjet printing of ultra-thin layers (< 100 nm) (see schematics in Figure 1). In the ink preparation phase, pgBTTT was dissolved in Cyrene, ultrasonicated (in an ultrasonic bath), and left to stir (≈300 rpm) on a hotplate at 30 – 35 °C for at least 24 h or until homogeneous solubilization was obtained followed by a dynamic viscosity measurement that indicated ≈16.5 cP (Figure S1 in the Supporting Information), thereby confirming the suitability of the ink for the inkjet printing process.

### 2.3. Inkjet Printing Conditions

Besides being a polar and high boiling point solvent, Cyrene is a good choice for the inkjet printing process due to its high density, allowing a reduction of the polymer concentration in the inks. The use of Cyrene-based inkjet ink formulations facilitates consistent drop formation and jetting behavior (Movie S1 in the Supporting Information), which leads to reliable drop-on-demand inkjet printing performance. The reason inkjet printing was selected as the deposition method is due to the low consumption of materials; only a few mg of semiconductor polymer is needed to prepare a few mL of the ink formulation. A printing resolution of 25 µm, or 1016 dots per inch, was employed to sequentially deposit either 2 or 4 layers of the semiconductor polymer material, forming the channel electrodes of the vertically stacked OECTs.

### 2.4. OECT Device Architectures

This study focused on using pgBTTT as the channel material in vertically stacked OECTs (**Figure 2**). The choice of the OECT architecture, co-planar or vertically stacked, is crucial and dictated by the intended application, e.g., biosensing, logic circuits, monitoring of electrophysiological signals, as well as the availability of deposition techniques.[14,16]

Figure 2a shows a cross–section of the OECT and Figure 2b shows a pictorial representation, including the electrical wires used for the voltage supply. A vertically stacked OECT typically consists of at least five subsequently printed layers. The printing process includes at least four screen printed layers (Ag interconnects, carbon-based source and drain electrodes, an optional insulating layer to minimize parasitic side reactions, electrolyte, the gate electrode, and an optional insulating layer for mechanical protection) and, in this work, an inkjet-printed layer of the pgBTTT-based OECT channel material. The combination of different printing technologies is beneficial to reach a good compromise between OECT performance (i.e., inkjet printing of thin and narrow channels implies shorter switching times and less energy consumption upon operating the OECTs) and process scalability/robustness (screen printing of less critical materials and dimensions). The solid electrolyte layer was deposited using an electrolyte ink formulation developed by RISE. This ink was developed initially for UV curing. However, due to the risk of degrading the semiconductor polymer upon UV light irradiation, as discussed in Figure S2 (Supporting Information), the screen-printed electrolyte was instead thermally cured using a convection oven.

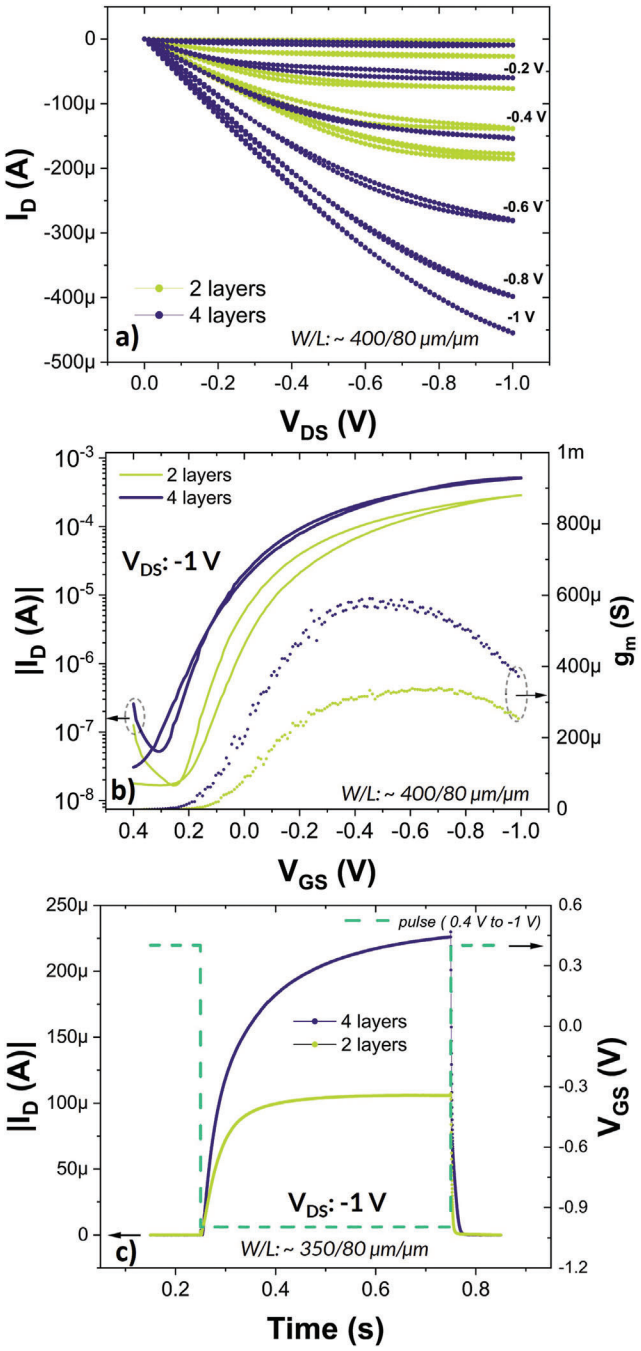


**Figure 4.** Electrical characterization of vertically stacked OECT devices. a) Output and b) transfer curves (drain current on the left y-axis and transconductance on the right y-axis) of vertically stacked OECTs with two and four inkjet printed pgBTTT-based channel layers. c) Transient measurements for the comparison of OECTs with different channel thicknesses.

**Figure 3** shows a photograph and microscope images of all-printed OECTs fabricated according to the vertically stacked de-

vice architecture. As shown in Figure 3a, the developed OECTs can be realized on polyethylene terephthalate (PET) substrates. Here, the devices are organized four by four to simplify the connections with the external addressing electronic circuits. PEDOT:PSS, screen printed on top of the electrolyte, serves as the gate electrode material in the OECT devices (see Figure 3b). The channel length of the all-printed OECTs is displayed in Figure 3c, indicating a channel width/length (W/L) ratio of ≈5 based on the approximate OECT channel dimensions of 350–400 µm ($W$) and ≈80 µm ($L$). A microscope image showing the cross–sectional view of the OECT is shown in Figure S3 (Supporting Information).

### 2.5. All-Printed Vertically Stacked OECTs

OECTs with pgBTTT as the channel material, manufactured in a co-planar arrangement via photolithography, have been previously demonstrated.[30] These devices showed superior figures of merit, i.e., high transconductance ($g_m = \frac{\partial I_D}{\partial V_G}$) ≈21 mS and mobility-capacitance product ($\mu C^*$) ≈502 F cm$^{-1}$ V$^{-1}$ s$^{-1}$; these values can be extracted from **Equation (1)**.

$$g_m = \frac{Wd}{L}\mu C^* \left|\left(V_T - V_G\right)\right| \quad (1)$$

$d$ denotes the thickness of the printed film serving as the OECT channel, $W$ and $L$ represent the lateral transistor channel dimensions, $\mu$ is the charge carrier mobility, $C^*$ is the volumetric capacitance, while $V_T$ and $V_G$ represent the threshold and gate voltages, respectively. The $\mu C^*$ product is the common (material-system) figure of merit that compares different organic mixed ionic-electronic conductors (OMIECs) used as the active OECT channel materials.[21,33] $g_m$ is an important device-system figure of merit, which depends on the thickness and area of the channel material of the OECT devices. It has been reported to scale linearly (e.g., in PEDOT:PSS-based OECTs) for low values of $WdL^{-1}$.[34] It is common to normalize $g_m$ to the thickness and the lateral dimensions (W and L) of the channel to acquire the ($g_{m,\,norm.} = g_m \frac{L}{Wd}$) performance metrics since this enables a comparison with other OMIECs. In OECTs with pgBTTT used as the channel material, applying a negative potential to the gate electrode facilitates hole accumulation in the bulk of the channel, while concurrently applying a negative $V_{DS}$, due to oxidation of the pgBTTT-based channel.[30]

The process flow (printing order) used in the manufacturing of the transistors is described in Figure S4 (Supporting Information). The printing order of the channel material (before or after screen printing the source and drain electrodes) had a significant effect on the OECT performance; Figure S4c,d (Supporting Information) shows that a change in the printing order of the channel material influences the OFF current values, thereby also affecting the ON–OFF ratio. The resulting OFF current values for OECTs with channels inkjet printed before and after screen printing the source and drain electrodes are ≈−40 nA and ≈−2.5 µA, respectively, which may be explained by the difference in uniformity of the inkjet-printed channel layers.

Further optimization of all-printed vertically stacked OECTs, by using an aspect ratio of ≈5 ($W/L$ = ≈400/80 µm), resulted in maximum values of $g_{m,\,norm}$ ≈12.9 mS cm$^{-1}$ and $\mu C^*$ ≈21 F cm$^{-1}$ V$^{-1}$ s$^{-1}$, and an ON–OFF ratio >10$^4$ (maximum ON current ≈−500 µA and minimum OFF current ≈−15 nA). The values are extracted from typical output and transfer curves, see **Figure 4a,b** and **Table 1**. The effect of the gate voltage ($V_{GS}$) sweeping range, i.e., from 0.2 to −1 V or from 0.4 to −1 V, during the OECT transfer measurements is demonstrated in Figure S5 (Supporting Information). The enlarged $V_{GS}$ range significantly reduced the OFF current value of the OECT comprising the thick channel layer from ≈−270 to ≈−50 nA. The relatively low $\mu C^*$, $g_{m,\,norm}$, and $g_m$ (Table 1), when compared to spin-coated OECTs (Table S1, Supporting Information), could be explained by the type of electrolyte being used (highly concentrated aqueous salt solutions are typically used in the reported literature); the screen printed and cured electrolyte layers result in lowered ionic conductivity, as compared to aqueous electrolytes.[30] Also, the resolution of the screen printing process limits the channel length to ≈80 µm in all-printed OECTs, in contrast to channel lengths of <10 µm achievable in OECTs manufactured by photolithography. Additionally, the use of screen-printed carbon-based source and drain electrodes increases the overall resistance of these OECT devices, which also contributes to the lowered transconductance.

In all-printed OECTs, a $W/L$ ratio of 10 can be reached by a two-fold increase of the channel width, i.e., from ≈400 to 800 µm. In this case, to enable efficient gating, the dimensions of the gate electrode need to be increased to achieve higher charge capacity.[21] However, these adaptations will come at the cost of a larger device footprint and longer switching times.

The effect of the solvent, i.e., Cyrene or chloroform, on the switching performance of the OECTs was assessed by conventional OECTs (spin-coated devices widely reported in the literature) with Au-based source and drain electrodes, Ag/AgCl gate electrodes and aqueous 0.1 M NaCl as the electrolyte. The OECTs exhibited similar transconductance and transfer behavior, as shown in Figure S6 (Supporting Information). It should be noted that W and L were fixed for both configurations, but the films had different thickness values (≈37 and ≈78 nm), which explains the difference in transconductance values and ON current levels. The variations in film thickness are explained by the different boiling points of the solvents, resulting in different drying behavior and rheological properties. This study resulted in OECTs with very good switching performances (e.g., transconductance and $\mu C^*$; see Table S1, Supporting Information), and the devices originating from the Cyrene-based solutions are performing almost equal with the devices spin-coated from chloroform after normalization of the transconductance (453 vs 687 S cm$^{-1}$). This is a significant result that justifies the choice of Cyrene as the solvent from a device standpoint, besides the environmental and safety benefits of this solvent.

The performance characteristics of OECTs with two different thicknesses (≈67 and ≈100 nm), which correspond to two (thin) and four (thick) inkjet printed layers, are summarized in Table 1. The increased number of layers in the thick OECTs results in higher $g_{m,\,norm}$, and $\mu C^*$ values but a lower ON–OFF ratio. It was

**Table 1.** OECT characteristics and figures of merit.

| pgBTTT | $g_{m}$ [mS] | $g_{m,\,norm}$ [S cm$^{-1}$] | $d$ [nm] | $I_{ON-OFF}$ | $V_T$ [mV] | $\mu C^*$ [Fcm$^{-1}$ V$^{-1}$ S$^{-1}$] |
|---|---|---|---|---|---|---|
| 2 layers | ≈0.32 ± 0.03 | 10.8 ± 1 | ≈67 | ≈16 100 ± 674 | ≈100 ± 9 | ≈15 ± 1 |
| 4 layers | ≈0.56 ±0.025 | 12.9 ± 0.6 | ≈100 | ≈8350 ± 2330 | ≈200 ± 40 | ≈21 ± 1.8 |

deduced from Figure 4b that the OECT with thin and thick channels exhibited OFF current values of ≈−16 and ≈−65 nA, respectively, leading to a higher ON–OFF ratio for the OECT with the thin channel. Both types of OECT devices (thin and thick channels) demonstrated device-to-device repeatability (Figures S7 and S8, Supporting Information) upon the refined fabrication process, i.e., inkjet printing the channel before screen printing the source and drain electrodes. The minor hysteresis that is observed in the transfer sweeps of the 2-layered OECT devices could be associated with a more non-uniform coverage when only two layers of the channel material are inkjet printed. In addition, Figure 4b shows lower OFF current levels for the 2-layered devices, at positive gate voltages, and this deeply reduced state may also result in a transfer behavior with more hysteresis.

OECTs manufactured on the same day but tested immediately or three days after manufacturing showed deviations in their ON current values; the ON current was ≈25% lower in the devices tested three days after manufacturing (Figure S9, Supporting Information). The devices were measured in ambient conditions, and due to the hygroscopic nature of the electrolyte layer, this deviation might be explained by slight variations in relative humidity levels at the different measurement occasions.

The transient behavior of $I_{DS}$ was investigated by pulsing $V_{GS}$ between 0.4 and −1 V, as demonstrated in Figure 4c. The all-printed pgBTTT-based OECTs exhibit a relatively fast switching response; rise ($t_r$) and fall ($t_f$) times were acquired with different channel thicknesses (thin; two layers and thick; four layers). These parameters define the time needed to reach 90% ($t_r$) and 10% ($t_f$) of the maximum ON current level, respectively. $t_r$ ≈105 ms and $t_f$ ≈5 ms were achieved for the OECTs with the thin channel, while the thick-layered OECTs resulted in $t_r$ ≈221 ms and $t_f$ ≈12 ms.

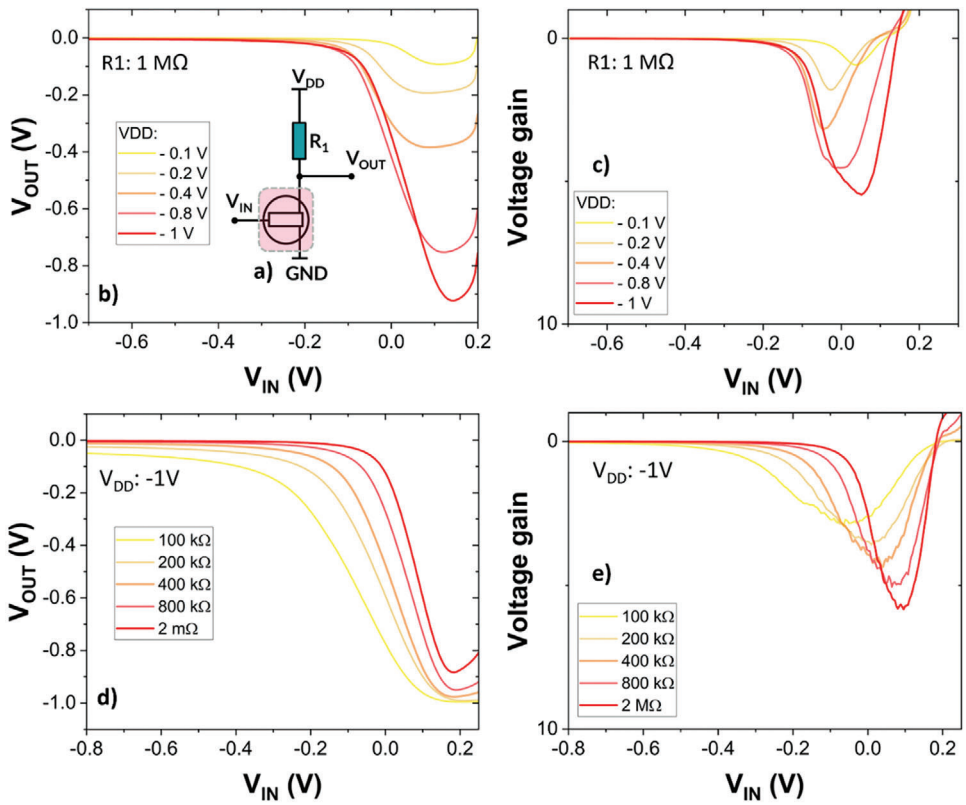


**Figure 5.** Measurements based on the conversion from the conventional OECT current modulation into voltage measurement mode. a) The voltage divider circuit determines the voltage amplification of the OECTs. b) Voltage transfer characteristics upon applying various $V_{DD}$ voltages (from −0.1 to −1 V) at constant $R_1$ (1 MΩ), and c) the corresponding voltage gain based on the same measurement. d) Voltage transfer characteristics upon varying the resistor values ($R_1$) in the range 100 kΩ - 2 MΩ at constant $V_{DD}$ (−1 V), and e) the corresponding voltage gain based on the same measurement.

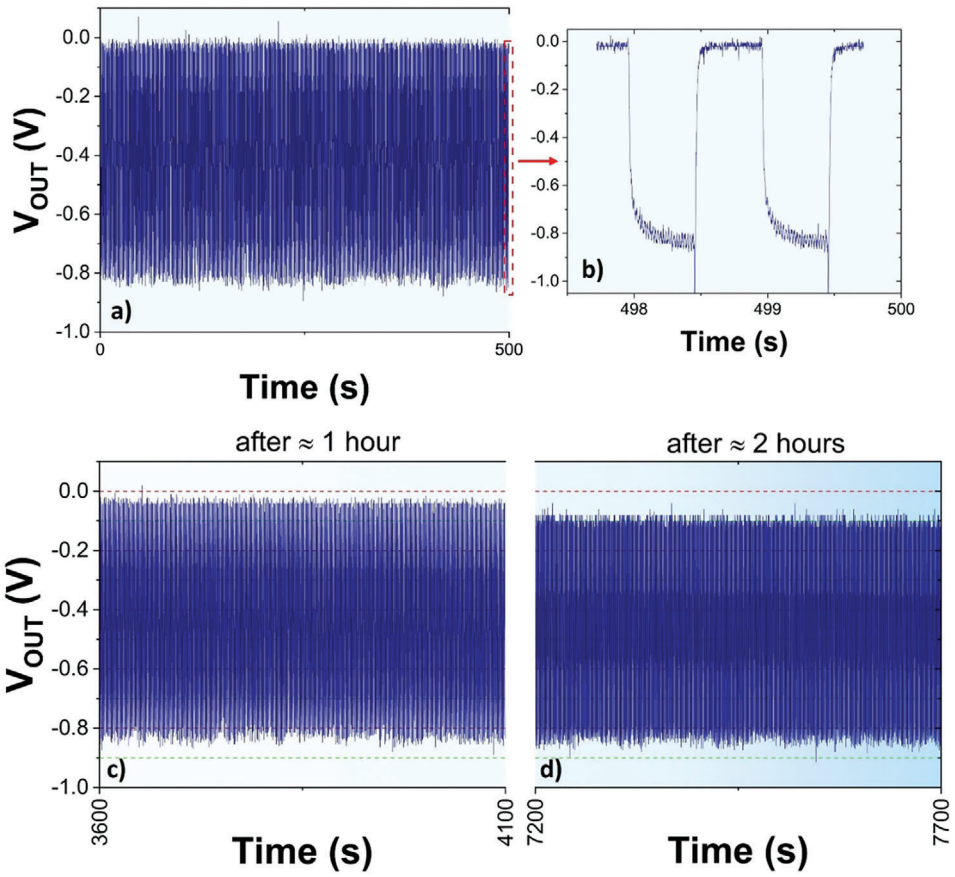


**Figure 6.** The operational stability of all-printed pgBTTT-based OECTs. a) Continuous OECT cycling by alternating $V_{IN}$ between −0.6 and 0.2 V at 1 Hz for 500 s, at a constant $V_{DD}$ of −0.9 V. b) Zoom-in of the output voltage signal during the final 5 s of the measurement in a). Only minor degradation is observed by the lowered output voltage amplitude after continuous OECT cycling for c) more than one hour and d) >2 h.

### 2.6. Voltage Divider Circuit to Determine OECT Voltage Amplification

The voltage divider circuit (**Figure** 5a) converts current into voltage at the output measurement node and assesses the voltage amplification in the all-printed OECTs with pgBTTT-based channels. In this measurement setup, the resistor ($R_1$) values ranged from 100 kΩ to 2 MΩ and the supply voltages ($V_{DD}$) ranged from −0.1 to −1 V.

As shown in Figure 5c, a maximum voltage gain of ≈5.5 is obtained using the highest $V_{DD}$ (−1 V) and a 1 MΩ resistor. Figure 5e shows a similar result; a maximum voltage gain of ≈5.8 is achieved for $R_1$ = 2 MΩ and a $V_{DD}$ of −1 V.

### 2.7. Operational Stability of All-Printed pgBTTT-based OECTs

The long-term operational stability of the all-printed pgBTTT-based OECTs was assessed by using the same voltage divider circuit (see **Figure** 6). $V_{DD}$ was set to −0.9 V and $R_1$ = 100 kΩ, while $V_{IN}$ was continuously alternated between −0.6 and 0.2 V at a frequency of 1 Hz for at least 2 h. As seen in Figure 6a, the OECT retained at least 99% of the output voltage range within the first 500 s of continuous cycling. The incorporation of the OECT in the voltage divider circuit (shown in Figure 5a) resulted in a switch-on time of ≈120 ms (down to −0.79 V) and a switch-off time of ≈20 ms (up to −0.09 V).[35] Figure 6c shows a voltage retention of ≈95% after one hour of continuous cycling, while Figure 6d demonstrates ≈91% voltage retention after 2 h of continuous cycling.

## 3. Conclusions

We have developed a novel ink formulation for inkjet printing in this work. The ink, based on the p-type semiconducting polymer pgBTTT, was further employed to fabricate the first all-printed vertically stacked OECTs operating in accumulation mode. The resulting devices exhibit good figures of merit and cycling stability. The novelty of the ink formulation originates from the utilization of the green solvent Cyrene to dissolve the pgBTTT serving as the OECT channels in the fabricated OECTs, as an alternative to the more toxic solvents that are commonly used, e.g., chloroform. Using biodegradable and bio-based solvents is advantageous in additive manufacturing, e.g., inkjet printing, to decrease the environmental impact of the ink preparation phase and the actual processing steps required for device fabrication. Moreover, from a device perspective, the obtained results also compare the performance metrics of conventional OECTs manufactured via

spin-coating to justify the use of Cyrene as a sustainable substitute for chloroform in the preparation of pgBTTT-based OECT devices. Overall, the results are very promising, and we envision these reproducible p-type accumulation mode all-printed pgBTTT-based OECTs to be further employed in all-printed complementary logic circuits.

## 4. Experimental Section

*Synthesis of pgBTTT*: The required monomers (see **1** and **2** in Figure S10 in the Supporting Information) were prepared according to literature procedures.[30,36] pgBTTT itself was synthesized according to an adapted literature protocol.[30] A dried schlenk tube was charged with stannylated thieno[3,2-*b*]thiophene **1** (71.8 mg, 154 µmol, 1 eq.), brominated bithiophene **2** (100 mg, 154 µmol, 1 eq.), tris(dibenzylideneacetone)dipalladium(0) (2.82 mg, 3.08 µmol, 0.02 eq.), tri(*o*-tolyl)phosphine (3.76 mg, 12.3 µmol, 0.08 eq.), and anhydrous DMF (3 mL). The schlenk tube was brought under an inert atmosphere by five vacuum/Ar cycles and was then heated to 100 °C for 16 h. Afterward, the mixture was diluted with DMF, the Pd scavenger diethylammonium diethyldithiocarbamate was added, and the mixture was stirred for 1 h at room temperature. The crude mixture was then added to methanol, after which the precipitate was subjected to Soxhlet extractions with methanol, acetone, hexanes, THF, and chloroform. The chloroform fraction was once again precipitated in methanol, filtered off, and dried under high vacuum. This resulted in 42.6 mg of pgBTTT (42% yield). MALDI-ToF mass spectrometry was carried out on this fraction, see Figure S11 in the Supporting Information.

*Fabrication of All-Printed OECTs*: OECTs were fabricated on 125 µm thick PET substrates (Polifoil from Policrom Screen) via a combination of screen and inkjet printing techniques. The PET substrates were thermally pre-treated (at 120 °C) before the device fabrication. Screen and inkjet printing was performed by a DEK Horizon 03iX screen printer and a Dimatix (DMP-2800) inkjet printer under ambient conditions (20–23 °C and 45–50 RH%). The polyester-based (mesh) screens were purchased from Marabu Scandinavia AB for the screen printing procedure. As shown in Figure 2a, the overall number of subsequently printed layers was five. A 2.4 pL cartridge (purchased from Fujifilm Dimatix) with a 1.5 mL cartridge reservoir and replaceable printhead for the inkjet printing process was utilized. The inkjet printing process was selected due to the low ink quantity (1.5 mL) and to minimize the waste of materials. The obtained ink dispersion was further filtered with a polypropylene filter membrane (0.22 µm) to ensure stable jetting and prevent nozzle clogging of the inkjet cartridge (Movie S1 in the Supporting Information). Either two or four OECT channel layers were subsequently printed without intermediate drying.

The typical printing order was the following: layer 1 - screen printing of Ag interconnects (Ag 5000 paste acquired from DuPont); layer 2 - inkjet printing of the pgBTTT-based channel; layer 3 - screen printing of the carbon-based (7102 paste purchased from DuPont) source and drain electrodes; layer 4 - screen printing of the electrolyte (E003, provided by RISE); layer 5 - screen printing of the gate electrode (the PEDOT:PSS-based screen printing paste Clevios S V4 purchased from Heraeus) on top of the electrolyte (Figure 3b). All layers were thermally cured using a convection or conveyor belt oven at a maximum temperature of 120 °C. The Cyrene solvent was purchased from Sigma-Aldrich.

Physical parameters, such as length (*L*), width (*W*), and thickness (*d*), were acquired via an optical microscope (Leica Microsystems) and a stylus profilometer (DektakXT). As shown in Figure S12 (Supporting Information), the average thickness for 1, 2, and 4 printed layers was estimated to be ≈48, ≈67, and ≈100 nm, respectively. The thicknesses of the screen-printed layers for Ag interconnects, carbon source and drain electrodes, and electrolytes were previously reported.[18]

*Fabrication of Conventional Spin-Coated OECTs*: Conventional OECT substrates were fabricated by thermal evaporation through a shadow mask on borosilicate glass. A 20 nm Cr adhesion layer followed by 80 nm of Au forms the source and drain electrodes. The channel material pgBTTT dissolved in chloroform (5 mg $mL^{-1}$ and stirred for >12 h at 40 °C) or in Cyrene (≈5 mg $mL^{-1}$, stirred for >12 h at 40 °C and 1 h at 120 °C) was subsequently spin-coated on the OECT substrate at 1000 rpm for 60 s. Due to the higher boiling point, the Cyrene-based OECTs were thermally annealed at 120 °C in order to evaporate the solvent. The Ag/AgCl gate electrode (A–M systems) was submerged in the 0.1 M NaCl electrolyte solution, which was contained within a PDMS well on top of the OECT channel.

The channel width was 6 mm, the channel lengths varied between 3, 2, 1, and 0.5 mm, and the channel thicknesses were acquired via a stylus profilometer (DektakXT). The average thicknesses are summarized in Table S1 (Supporting Information).

*The Viscosity of pgBTTT-Based Inkjet Ink*: The measurements indicated a dynamic viscosity of ≈16.5 cP (averaged) for ≈1.1 mg $mL^{-1}$ pgBTTT-based inkjet printing ink dissolved in Cyrene. The viscosity was acquired by a modular compact rheometer (Anton Paar MCR 102) with a rheometer cone CP50-1.

*Electrical Characterization of All-Printed OECTs*: The OECT devices were characterized under ambient conditions: 20–23 °C and 45–50 RH%. The output ($I_D$ vs $V_D$), transfer ($I_D$ vs $V_G$), and transient measurements ($I_D$ vs time) were performed using a digital storage oscilloscope (DSOX1204G from Keysight) and two different parameter analyzers (HP/Agilent 4155B and Keithley 4200A-SCS). In the output measurements, $V_{GS}$ was increased in steps of 200 mV, from 0 to −1 V, while $V_{DS}$ was swept from 0 to −1 V. For the transfer sweeps, a constant $V_D$ of −1 V was applied, while $V_{GS}$ was swept between 0.4 and −1 V in both directions. For the transient measurements, $I_D$ was recorded as a function of time; $V_{GS}$ was alternated between 0.4 and −1 V (square wave). In transient measurements, including the voltage divider circuit, $V_{DD}$ was set to −0.9 V and $V_{IN}$ was swept from −0.6 to 0.2 V at a frequency of 1 Hz for at least 2 h. A resistor ($R_1$) of 100 kΩ was used in the voltage divider circuit, and the measurements were performed under ambient conditions (20–23 °C and 45–50 RH%).

*Electrical Characterization of Conventional Spin-Coated OECTs*: The transfer curve measurements ($I_D$ vs $V_{GS}$) were performed using two Keithley 2400 source meters, controlled by custom LabView software. A constant $V_D$ of −0.7 V was applied, while $V_{GS}$ was swept between 0 and −0.7 V. Given the slight roughness of the measured transfer curves, smoothening was applied in order to consistently and more accurately extract the performance parameters of the OECT devices, such as the transconductance and the mobility-capacitance product. The smoothening of both the measured drain current and the gate voltage was applied by taking a moving average with a window size that was 20% of the original number of data points.

## Supporting Information

Supporting Information is available from the Wiley Online Library or from the author.

## Acknowledgements

This project received funding from the European Union's Horizon 2020 research and innovation program under grant agreement no. 964677 (MITICS). The authors would like to thank Jessica Åhlin for valuable electrolyte discussions. A.M. and P.A.E. thank Vinnova for financial support (grant agreement no. 2023-01337). W.M., L.B., and A.G. thank the FWO Vlaanderen for financial support (WEAVE project G025922N and Ph.D. grant 1S70122N).

## Conflict of Interest

The authors declare that they have no conflict of interest.

## Data Availability Statement

The data that support the findings of this study are openly available in Zenodo at https://doi.org/10.5281/zenodo.10792640.

## Keywords

green solvents, OECT, pgBTTT, printed electronics, sustainable

Received: November 23, 2023
Revised: February 14, 2024
Published online: March 11, 2024

[1] Y. Khan, A. Thielens, S. Muin, J. Ting, C. Baumbauer, A. C. Arias, *Adv. Mater.* **2019**, *32*, 1905279.
[2] M. J. Tan, C. Owh, P. L. Chee, A. K. K. Kyaw, D. Kai, X. J. Loh, *J. Mater. Chem. C* **2016**, *4*, 5531.
[3] M. Shahabuddin, M. Nur Uddin, J. I. Chowdhury, S. F. Ahmed, M. N. Uddin, M. Mofijur, M. A. Uddin, *Int. J. Environ. Sci. Technol.* **2023**, *20*, 4513.
[4] S. Chen, A. Surendran, X. Wu, S. Y. Lee, M. Stephen, W. L. Leong, *Adv. Mater. Technol.* **2020**, *5*, 2000523.
[5] P. Andersson Ersman, R. Lassnig, D. Tu, V. Keshmiri, R. Forchheimer, S. Fabiano, G. Gustafsson, M. Berggren, *Nat. Commun.* **2019**, *10*, 5053.
[6] H. Sun, M. Vagin, S. Wang, X. Crispin, R. Forchheimer, M. Berggren, S. Fabiano, *Adv. Mater.* **2018**, *30*, 1704916.
[7] M. Massetti, S. Zhang, H. Padinare, B. Burtscher, C. Diacci, D. T. Simon, X. Liu, M. Fahlman, D. Tu, M. Berggren, S. Fabiano, *npj Flexible Electron.* **2023**, *7*, 11.
[8] X. Gu, S. Y. Yeung, A. Chadda, E. N. Y. Poon, K. R. Boheler, I. M. Hsing, *Adv. Biosyst.* **2019**, *3*, 1800248.
[9] M. Braendlein, T. Lonjaret, P. Leleux, J. M. Badier, G. G. Malliaras, *Adv. Sci.* **2016**, *4*, 1600247.
[10] D. Khodagholy, T. Doublet, P. Quilichini, M. Gurfinkel, P. Leleux, A. Ghestem, E. Ismailova, T. Hervé, S. Sanaur, C. Bernard, G. G. Malliaras, *Nat. Commun.* **2013**, *4*, 1575.
[11] D. Khodagholy, J. N. Gelinas, Z. Zhao, M. Yeh, M. Long, J. D. Greenlee, W. Doyle, O. Devinsky, G. Buzsáki, *Sci. Adv.* **2016**, *2*, e1601027.
[12] B. Burtscher, P. A. Manco Urbina, C. Diacci, S. Borghi, M. Pinti, A. Cossarizza, C. Salvarani, M. Berggren, F. Biscarini, D. T. Simon, *Adv. Healthcare Mater.* **2021**, *10*, 2100955.
[13] A. Makhinia, P. Azizian, V. Beni, J. Casals-Terré, J. M. Cabot, P. Andersson Ersman, *Adv. Mater. Technol.* **2023**, *8*, 2300127.
[14] M. Galliani, C. Diacci, M. Berto, M. Sensi, V. Beni, M. Berggren, M. Borsari, D. T. Simon, F. Biscarini, C. A. Bortolotti, *Adv. Mater. Interfaces* **2020**, *7*, 2001218.
[15] A. Marks, S. Griggs, N. Gasparini, M. Moser, *Adv. Mater. Interfaces* **2022**, *9*, 2102039.
[16] P. Gkoupidenis, D. A. Koutsouras, G. G. Malliaras, *Nat. Commun.* **2017**, *8*, 15448.
[17] U. Boda, I. Petsagkourakis, V. Beni, P. Andersson Ersman, K. Tybrandt, *Adv. Mater. Technol.* **2023**, *8*, 2300127.
[18] A. Makhinia, K. Hübscher, V. Beni, P. Andersson Ersman, *Adv. Mater. Technol.* **2022**, *7*, 2200153.
[19] M. Zabihipour, R. Lassnig, J. Strandberg, M. Berggren, S. Fabiano, I. Engquist, P. Andersson Ersman, *npj Flexible Electron.* **2020**, *4*, 15.
[20] P. Andersson Ersman, D. Nilsson, J. Kawahara, G. Gustafsson, M. Berggren, *Org. Electron.* **2013**, *14*, 1276.
[21] J. Rivnay, S. Inal, A. Salleo, R. M. Owens, M. Berggren, G. G. Malliaras, *Nat. Rev. Mater.* **2018**, *3*, 17086.
[22] C. Y. Yang, M. A. Stoeckel, T. P. Ruoko, H. Y. Wu, X. Liu, N. B. Kolhe, Z. Wu, Y. Puttisong, C. Musumeci, M. Massetti, H. Sun, K. Xu, D. Tu, W. M. Chen, H. Y. Woo, M. Fahlman, S. A. Jenekhe, M. Berggren, S. Fabiano, *Nat. Commun.* **2021**, *12*, 2354.
[23] S. Zhang, P. Ding, T.-R. Ruoko, R. Wu, M. A. Stoeckel, M. Massetti, T. Liu, M. Vagin, D. Meli, R. Kroon, J. Rivnay, S. Fabiano, *Adv. Funct. Mater.* **2023**, *33*, 2302249.
[24] H. Y. Wu, J. D. Huang, S. Y. Jeong, T. Liu, Z. Wu, T. van der Pol, Q. Wang, M. A. Stoeckel, Q. Li, M. Fahlman, D. Tu, H. Y. Woo, C. Y. Yang, S. Fabiano, *Mater. Horiz.* **2023**, *10*, 4213.
[25] C. Y. Yang, D. Tu, T. P. Ruoko, J. Y. Gerasimov, H. Y. Wu, P. C. Harikesh, M. Massetti, M. A. Stoeckel, R. Kroon, C. Muller, M. Berggren, S. Fabiano, *Adv. Electron. Mater.* **2022**, *8*, 2100907.
[26] J. T. Friedlein, R. R. McLeod, J. Rivnay, *Org. Electron.* **2018**, *63*, 398.
[27] S. Chen, A. Surendran, X. Wu, S. Y. Lee, M. Stephen, W. L. Leong, *Adv. Mater. Technol.* **2020**, *5*, 2000523.
[28] Y. He, N. A. Kukhta, A. Marks, C. K. Luscombe, *J. Mater. Chem. C* **2022**, *10*, 2314.
[29] S. Moro, N. Siemons, O. Drury, D. A. Warr, T. A. Moriarty, L. M. A. Perdigão, D. Pearce, M. Moser, R. K. Hallani, J. Parker, I. Mcculloch, J. M. Frost, J. Nelson, G. Costantini, *ACS Nano* **2022**, *16*, 21303.
[30] R. K. Hallani, B. D. Paulsen, A. J. Petty II, R. Sheelamanthula, M. Moser, K. J. Thorley, W. Sohn, R. B. Rashid, A. Savva, S. Moro, J. P. Parker, O. Drury, M. Alsufyani, M. Neophytou, J. Kosco, S. Inal, G. Costantini, J. Rivnay, I. McCulloch, *J. Am. Chem. Soc.* **2021**, *143*, 11007.
[31] N. Turetta, W. Danowski, L. Cusin, P. A. Livio, R. Hallani, I. McCulloch, P. Samorì, *J. Mater. Chem. C* **2023**, *11*, 7982.
[32] S. Griggs, A. Marks, D. Meli, G. Rebetez, O. Bardagot, B. D. Paulsen, H. Chen, K. Weaver, M. I. Nugraha, E. A. Schafer, J. Tropp, C. M. Aitchison, T. D. Anthopoulos, N. Banerji, J. Rivnay, I. McCulloch, *Nat. Commun.* **2022**, *13*, 7964.
[33] M. Shahi, V. N. Le, P. Alarcon Espejo, M. Alsufyani, C. J. Kousseff, I. McCulloch, A. F. Paterson, *Nat. Mater.* **2023**, *23*, 2.
[34] D. Ohayon, V. Druet, S. Inal, *Chem. Soc. Rev.* **2023**, *52*, 1001.
[35] P. K. Madathil, S. Cho, S. Choi, T. D. Kim, K. S. Lee, *Macromol. Res.* **2018**, *26*, 934.
[36] C. Hütter, T. Rothländer, A. Haase, G. Trimmel, B. Stadlober, *Appl. Phys. Lett.* **2013**, *103*, 043308.